5th GRACM International Congress on Computational Mechanics
Limassol, 29 June – 1 July, 2005

ULTIMATE STRENGTH ANALYSIS OF ARBITRARY CROSS SECTIONS UNDER BIAXIAL BENDING AND AXIAL LOAD BY FIBER MODEL AND CURVILINEAR POLYGONS

Aristotelis E. Charalampakis and Vlasis K. Koumousis

Institute of Structural Analysis and Aseismic Research
National Technical University of Athens
NTUA, Zografou Campus GR-15773, Athens, Greece
e-mail: vkoum@central.ntua.gr, web page: http://users.ntua.gr/vkoum

Keywords: biaxial bending, fiber model, failure surface, composite structure.

Abstract. *A precise fiber model algorithm for the analysis of arbitrary cross sections under biaxial bending and axial load is presented. The method can be applied to complex cross sections of irregular shape and curved edges, with/without openings and consisting of various nested materials. The only assumption is that plane sections before bending remain plane after bending (Bernoulli – Euler assumption). The cross section is described by curvilinear polygons. The material properties are user – defined; the stress – strain diagrams of all materials are composed of any number and any combination of consecutive polynomial segments (up to cubic), subject to a desired accuracy. Various effects such as concrete confinement, concrete tensile strength, strain hardening of the reinforcement etc. may be taken into account. Apart from ultimate strength analyses, the algorithm can be applied to various other problems in which the Bernoulli – Eyler assumption holds, as demonstrated in a number of examples. A special purpose computer program with full graphical interface has been developed.*

1 INTRODUCTION

The analysis of an arbitrary cross-section under biaxial bending and axial load has received extensive attention in the literature lately [6], [4], [9]. With the advent of inexpensive computer systems, the generation of the failure surface has been made possible using the "fiber" approach. This approach produces consistent results that agree closely with experimental results [2].

The failure of the cross section corresponds to the top of the moment – curvature diagram. However, the conventional failure, defined by design codes, occurs when any of the materials reaches its predefined maximum allowable strain, either compressive or tensile.

This kind of analyses is important since it is used by the Codes. Also, the failure surface is important for non-linear analyses since the plastic deformations of a structural element are functions of the load history and the distance of the load vector from the surface. Moreover, it provides grounds for a damage analysis of the cross section.

2 GENERATION OF FAILURE SURFACE

There are three different techniques to generate the failure surface of an arbitrary cross section: (1) interaction curves for a given bending moments ratio, (2) load contours for a given axial load and (3) isogonic or 3D curves.

The first two techniques require the calculation of the position of the neutral axis. The set of equilibrium equations are non linear and coupled, and an iterative approach such as the quasi-Newton method proposed by Yen [10], is needed to determine the position of the neutral axis. These procedures are not straightforward to implement and, in many cases, are sensitive to the selection of the origin of the reference system. These algorithms usually become unstable near the state of pure compression.

On the other hand, the third technique, which is used in the method presented, is more direct because the direction of the neutral axis is assumed from the very beginning. The produced points describe a more complex 3D plot, because the meridians, in general, are not plane. This is due to the asymmetry of the cross section, as described later.

3 CROSS SECTION

The curvilinear polygon is the only type of graphical object that is used for the description of all cross

sections. A curvilinear polygon has edges that may be straight lines and/or arcs. Since these polygons can be nested in any depth, it is obvious that almost any cross section can be described accurately. Circles are taken into account as two-sided curvilinear polygons with curved edges. Note that even small objects, such as the reinforcement bars, are treated as actual graphical objects and not dimensionless individual fibers.

In order to significantly reduce the expensive calculations required to identify the various regions in a complex cross section with nested materials, each curvilinear polygon is treated separately. Two material properties are defined: the "foreground" material and the "background" material. The foreground material is taken into account with a positive sign during the integration of the stresses, whereas the background material is taken into account with a negative sign. Therefore, almost any cross section can be described, as shown in the example of Figure 1:

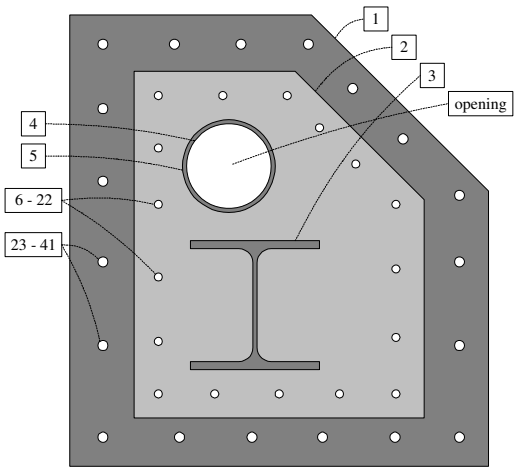

Object	Number of Nodes	Foreground material	Background material
1	5	Unconfined (outer) concrete	None
2	5	Confined (inner) concrete	Unconfined (outer) concrete
3	16	Structural steel	Confined (inner) concrete
4	2	None	Structural steel
5	2	Structural steel	Confined (inner) concrete
6 - 22	2	Reinforcement	Confined (inner) concrete
23 - 41	2	Reinforcement	Unconfined (outer) concrete

Figure 1. Example of complex cross section and nested materials

4 MATERIAL PROPERTIES

The stress – strain diagrams of all materials are composed of any number and any combination of consecutive segments. Each segment is a polynomial expression (up to cubic), which is automatically defined by an appropriate number of points; for example, a cubic segment is defined by four consecutive points. Therefore, the stress strain diagrams of a certain kind of concrete and steel may be defined as shown in Figure 2:

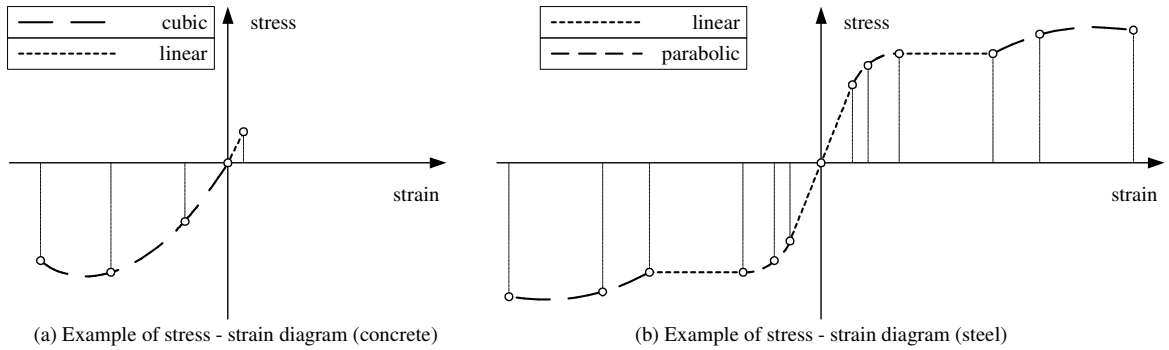

(a) Example of stress - strain diagram (concrete)

(b) Example of stress - strain diagram (steel)

Figure 2. Example of stress – strain diagrams (tension positive)

Apart from the stress – strain diagram, the material structure holds data related to the maximum compressive and tensile strain and whether reach of these values signifies the conventional failure of the cross section.

5 CALCULATIONS

5.1 Rotation

We assume that the X axis is parallel to the longitudinal dimension of the element. Any convenient point may be used as origin for the calculations. Since the direction of the neutral axis is assumed from the beginning, it is

convenient to express all coordinates in another YZ Cartesian system with Y axis parallel to the neutral axis. Therefore, the Cartesian system is rotated counter-clockwise around the origin by an angle θ, as shown in Figure 3.

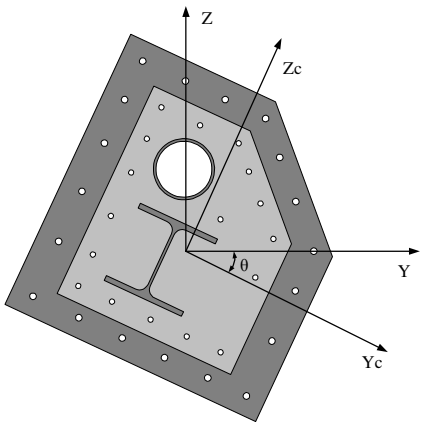

Figure 3. Rotation of cross section

$$\begin{bmatrix} Y \\ Z \end{bmatrix} = \begin{bmatrix} \cos(\theta) & \sin(\theta) \\ -\sin(\theta) & \cos(\theta) \end{bmatrix} \cdot \begin{bmatrix} Y_c \\ Z_c \end{bmatrix} \tag{1}$$

In this way, the strains and therefore the stresses vary only in Z axis.

5.2 Decomposition of curvilinear polygons

The next step is the decomposition of all curvilinear polygons into curvilinear trapezoids. The top and bottom edges of the curvilinear trapezoids are straight lines parallel to the neutral axis whereas the left and right edges may be straight lines or arcs. This procedure needs to be done only once for each assumed direction of the neutral axis; this basic set of trapezoids may be stored in memory and retrieved when needed.

Figure 4 shows an example of decomposition of a steel section and some of the produced curvilinear trapezoids. Note that the section is described exactly by a 16-node curvilinear polygon:

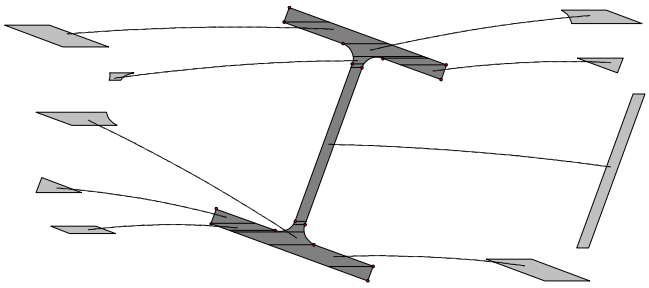

Figure 4. Decomposition of a steel section into curvilinear trapezoids

For reasons of simplicity we will drop the term “curvilinear” for both the curvilinear polygons and the curvilinear trapezoids.

5.3 Calculation of integrals

The next step is the calculation of the basic integrals of the trapezoids. These integrals are of the form $y^m \cdot z^n$, where m, n, specific integers (equation (2)). The expressions for the integrals are analytical. Again, the integrals need to be evaluated only once for each assumed direction of the neutral axis; the results can be stored in memory and retrieved when needed. Therefore, the overhead for using analytical expressions is minimal.

$$I^j_{(m,n)} = \int_{trapezoid\ j} \left(y^m \cdot z^n \right)$$
$$(m,n) = (0,0..4),\ (1,1..4) \tag{2}$$

This technique is also used for the exact calculation of cross sectional properties, such as area, first moments of area, centroids, moment of inertia, products of inertia, principal axes etc.

5.4 Strain distribution

We assume that plane sections remain plane; therefore we need three parameters to define the deformed plane. The first parameter is the direction of the neutral axis; we have already taken advantage of this by rotating the cross section. The other two parameters are the curvature k and the strain ε_0 at the origin; as mentioned earlier, the strain is a function of z only (equation (3)):

$$\varepsilon(z) = \varepsilon_0 + k \cdot z \tag{3}$$

Given k, ε_0, the neutral axis is a line parallel to the Y axis at a distance given by equation (4):

$$z_{na} = -\frac{\varepsilon_0}{k} \tag{4}$$

5.5 Calculation of stress resultants

The calculation of stress resultants will take place for an imposed deformed configuration defined by a set of given θ, k, ε_0. In general, we assume that the segment of the stress – strain diagram covering the specific trapezoid is a cubic polynomial expression (equation (5)):

$$\sigma(\varepsilon) = \sum_{i=0}^{3}\left(a_i \cdot \varepsilon^i\right) \tag{5}$$

The coefficients α_i are known and constant properties of the material. Substituting (3) into (5) we obtain:

$$\begin{aligned}
&\sigma(k,\varepsilon_0,z) = \sum_{i=0}^{3}\left(b_i \cdot z^i\right)\\
&b_0 = \alpha_3 \cdot {\varepsilon_0}^3 + \alpha_0 + \alpha_1 \cdot \varepsilon_0 + \alpha_2 \cdot {\varepsilon_0}^2\\
&b_1 = 3 \cdot \alpha_3 \cdot {\varepsilon_0}^2 \cdot k + 2 \cdot \alpha_2 \cdot \varepsilon_0 \cdot k + \alpha_1 \cdot k\\
&b_2 = 3 \cdot \alpha_3 \cdot \varepsilon_0 \cdot k^2 + \alpha_2 \cdot k^2\\
&b_3 = \alpha_3 \cdot k^3
\end{aligned} \tag{6}$$

The stress resultants of trapezoid j are calculated by integration of equation (6):

$$N_x^j = \int_{trapezoid\ j}\left(\sum_{i=0}^{3}\left(b_i \cdot z^i\right)\right) = \sum_{i=0}^{3}\left(b_i \cdot \int_{trapezoid\ j}\left(z^i\right)\right) = \sum_{i=0}^{3}\left(b_i \cdot I_{(0,i)}^j\right) \tag{7}$$

$$M_y^j = \int_{trapezoid\ j}\left(\sum_{i=0}^{3}\left(b_i \cdot z^i\right) \cdot z\right) = \sum_{i=0}^{3}\left(b_i \cdot \int_{trapezoid\ j}\left(z^{i+1}\right)\right) = \sum_{i=0}^{3}\left(b_i \cdot I_{(0,i+1)}^j\right) \tag{8}$$

$$M_z^j = \int_{trapezoid\ j}\left(\sum_{i=0}^{3}\left(b_i \cdot z^i\right) \cdot y\right) = \sum_{i=0}^{3}\left(b_i \cdot \int_{trapezoid\ j}\left(z^i \cdot y\right)\right) = \sum_{i=0}^{3}\left(b_i \cdot I_{(1,i)}^j\right) \tag{9}$$

$$\begin{aligned}
c_y^j &= M_z^j \Big/ N_x^j\\
c_z^j &= M_y^j \Big/ N_x^j
\end{aligned} \tag{10}$$

In equation (10), c_y^j, c_z^j are the coordinates of the central axis of N_x^j. Note that the integrals $I_{(m,n)}^j$ are already calculated and are independent of k, ε_0. By a simple summation of the stress resultants of all trapezoids, we obtain the overall forces and bending moments required to impose the specific deformed configuration. To summarize:

- Pick k, ε_0.

- For trapezoid j:
  Since α_i are known, calculate b_i (equations (6))
  Since $I_{(m,n)}^{j}$ are known, calculate the stress resultants (equations (7) to (10)).
- Sum the results from all trapezoids to obtain overall results N_X, M_Y, M_Z.

6 CONSTRUCTION OF MOMENT-CURVATURE DIAGRAM

For a specified axial load and direction of neutral axis (angle θ) , a full moment – curvature diagram can be constructed. After the initialization (rotation of cross section, decomposition of polygons into trapezoids, calculation of the basic integrals of the trapezoids), small increments of Δk are applied as imposed curvature. Since the curvature k is given, the algorithm uses a fast Van Wijngaarden – Dekker – Brent method to evaluate the strain ε_0 at the origin in order to achieve axial equilibrium to a specified accuracy.

As the curvature increases, the neutral axis moves perpendicular to its direction. This incremental procedure continues until the moment reaches a maximum (failure) or until one of the materials reaches the maximum compressive or tensile strain specified by the user (conventional failure). Thus, the complete moment – curvature diagram can be obtained, both for the primary moment M_Y and for secondary moment M_Z. In general, the secondary moment M_Z, expressed by equation (9), is small compared to the primary moment M_Y.

Finally, the moments can be expressed in the global reference system with an inverse rotational transformation:

$$\begin{bmatrix} M_{Yc} \\ M_{Zc} \end{bmatrix} = \begin{bmatrix} \cos(\theta) & -\sin(\theta) \\ \sin(\theta) & \cos(\theta) \end{bmatrix} \cdot \begin{bmatrix} M_Y \\ M_Z \end{bmatrix} \tag{11}$$

The algorithm uses a variable curvature step which is adjusted automatically; therefore, the final result is independent of the initial curvature step (specified by the user). A small initial curvature step produces a smooth moment – curvature diagram.

7 CONSTRUCTION OF INTERACTION CURVES AND FAILURE SURFACES

By repeating the procedure described previously for different directions θ of the neutral axis in the range of 0^0 – 360^0, we are able to construct the interaction curve for a given axial load. Next, by constructing interaction curves for various axial loads, we are able to construct the full failure surface of the cross section equator – by – equator.

8 DEFORMED CONFIGURATION UNDER GIVEN LOADS

The algorithm can be used for calculating the deformed configuration of a cross section under given loads. The calculation is a trial and error procedure (Figure 5). The task is to calculate the parameters θ, k, ε_0 defining the deformed plane for which the cross section is in equilibrium with the external loads N_{Xc}^{T}, M_{Yc}^{T}, M_{Zc}^{T}.

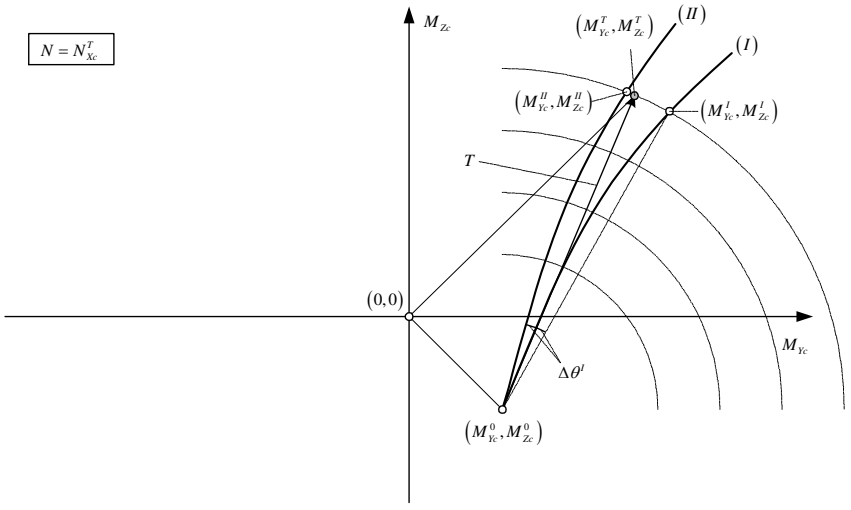

Figure 5. Calculation of deformed configuration under given loads

All calculations are performed with axial load equal to N_{Xc}^{T}. The origin can be any point therefore, we first have to calculate the bending moments M_{Yc}^{0}, M_{Zc}^{0} required for a deformed plane with no curvature (k=0). Since curvature is always increased from zero until failure is achieved, these bending moments is the first pair of results for any direction θ of the neutral axis. Therefore, the paths of all analyses stem from (M_{Yc}^{0}, M_{Zc}^{0}). The target vector T connects (M_{Yc}^{0}, M_{Zc}^{0}) with (M_{Yc}^{T}, M_{Zc}^{T}).

As first attempt (I), we set the direction θ^{I} of the neutral axis equal to the direction of the target vector T. As curvature is increased, the path of the analysis deviates because of the secondary moment M_Z; when the norm reaches the norm of the target vector, the analysis stops and the result (M_{Yc}^{I}, M_{Zc}^{I}) may differ from the target values (M_{Yc}^{T}, M_{Zc}^{T}). The direction of the neutral axis is then corrected by the difference $\Delta\theta^{I}$ found in the first iteration. In the second attempt, the results (M_{Yc}^{II}, M_{Zc}^{II}) are much closer to the target values. The procedure stops when a specified accuracy is achieved.

8 COMPUTER IMPLEMENTATION

A computer program, called myBiAxial, which implements the method presented, has been developed. The program features a full graphical interface. It is also capable of importing cross sectional data from DXF files. Some screen shots are shown in Figure 6:

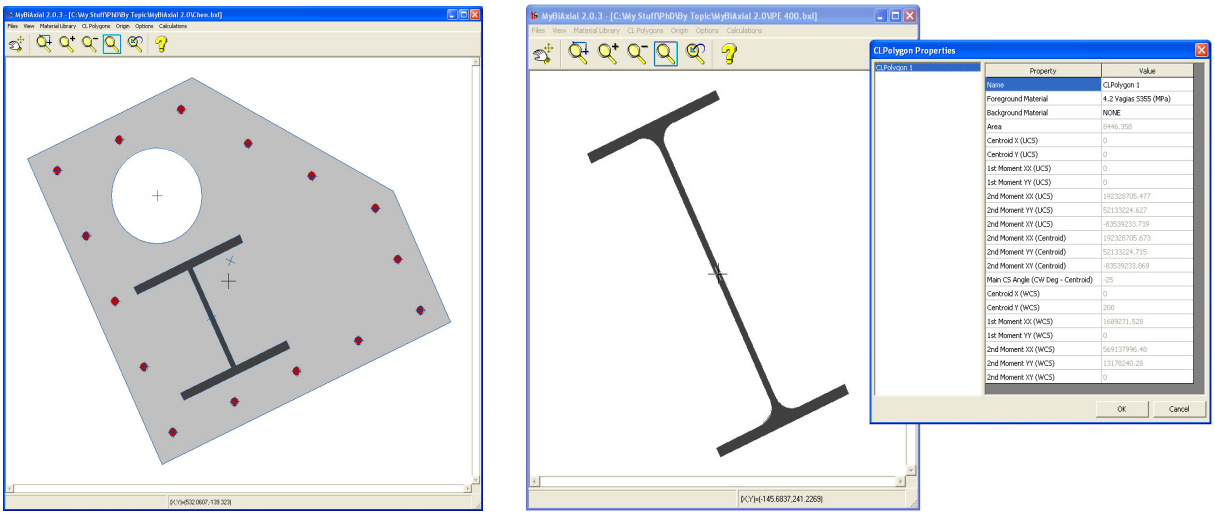

(a) (b)

Figure 6. MyBiAxial computer program

9 VALIDATION - EXAMPLES

9.1 Example 1

Eurocode 2 provides design charts for common reinforced concrete cross sections. These charts provide combinations of axial loads and their respective ultimate bending moment capacities (which correspond to the conventional failure of the cross section), for a range of longitudinal reinforcement expressed by the mechanical reinforcement percentage ω (equation (12)).

$$\omega = \frac{A_{s,tot}}{A_{c,tot}} \cdot \frac{f_{yd}}{f_{cd}} \tag{12}$$

where $A_{s,tot}$ is the total area of longitudinal reinforcement, $A_{c,tot}$ is the total area of concrete, f_{yd}, f_{cd} are the design strengths of steel and concrete respectively. Also, the axial load and bending moment are normalized with respect to the concrete properties and the cross sectional dimensions (equation (13)); therefore, a single chart covers all cases for a certain steel grade.

$$\nu = \frac{N_d}{A_{c,tot} \cdot f_{cd}}$$
$$\mu = \frac{M_d}{A_{c,tot} \cdot h \cdot f_{cd}} \tag{13}$$

Eurocode 2 specifies the value of 0.020 as the ultimate strain limit for longitudinal steel reinforcement. Also, for large compressive axial loads, it reduces the ultimate curvature capacity by imposing the rotation of the strain profile around point C which is located at a distance 3/7·h from the most compressed fiber and has a strain of ε_0=-0.002. This restriction is included easily in the algorithm; however, it is of little practical interest since large compressive axial loads in concrete cross sections must be avoided for other reasons i.e. creep.

The developed computer program was used to calculate pairs of axial loads and bending moments for the rectangular cross section of Figure 7a. The characteristic strengths and partial safety factors for concrete and reinforcement bars were taken as follows:

$$f_{ck} = 20MPa, \gamma_c = 1.5$$
$$f_y = 500MPa, \gamma_r = 1.15$$

Five different cases of longitudinal reinforcement were considered, i.e. ω=0.00, 0.50, 1.00, 1.50, 2.00. The computed results, summarized in Table 1, follow the corresponding curve exactly, as shown in Figure 7c.

ν	μ (ω=0.00)	μ (ω=0.50)	μ (ω=1.00)	μ (ω=1.50)	μ (ω=2.00)
1.60					0.1607
1.40				0.0402	0.2408
1.20				0.1203	0.3219
1.00				0.2007	0.4031
0.80			0.0801	0.2823	0.4841
0.60			0.1613	0.3636	0.5645
0.40		0.0400	0.2433	0.4440	0.6441
0.20		0.1228	0.3237	0.5232	0.7230
0.00	0.0000	0.2031	0.4020	0.6015	0.8016
-0.10	0.0424	0.2412	0.4406	0.6402	0.8397
-0.20	0.0746	0.2748	0.4739	0.6728	0.8717
-0.30	0.0951	0.2939	0.4920	0.6903	0.8883
-0.35	0.1010	0.2988	0.4967	0.6944	0.8919
-0.40	0.1033	0.2943	0.4883	0.6828	0.8775
-0.60	0.0824	0.2465	0.4287	0.6176	0.8091
-0.80	0.0193	0.1938	0.3690	0.5526	0.7409
-1.00		0.1292	0.3072	0.4875	0.6729
-1.20		0.0548	0.2406	0.4214	0.6047
-1.40			0.1670	0.3525	0.5358
-1.60			0.0897	0.2792	0.4652
-1.80				0.2030	0.3921
-2.00				0.1245	0.3159
-2.20					0.2384
-2.40					0.1595

Table 1. Computed results

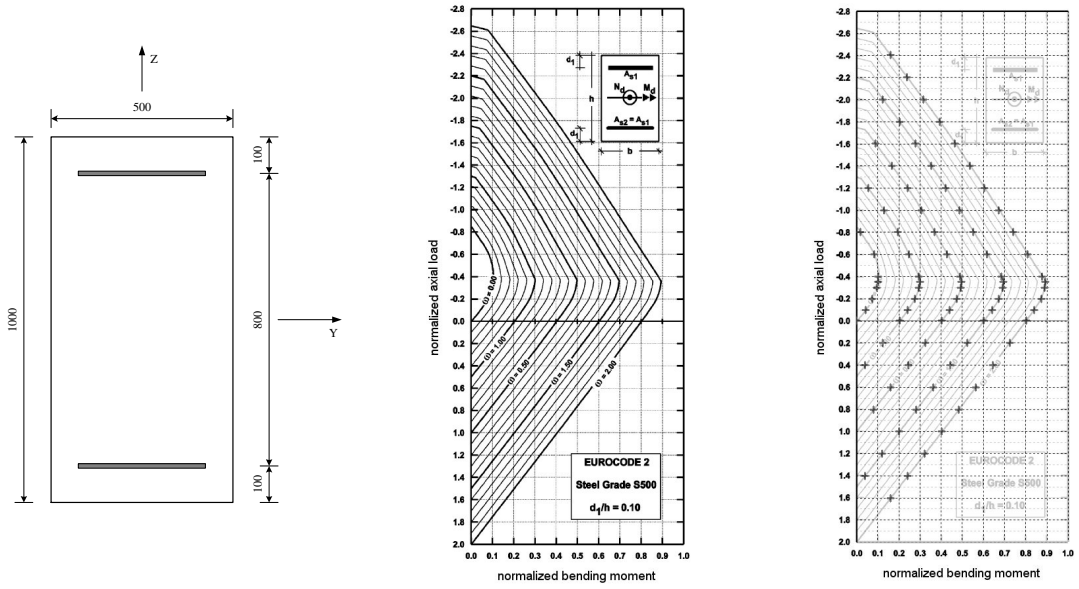

(a) (b) (c)

Figure 7. (a) Rectangular reinforced concrete cross section (distances in mm)
(b) Corresponding EC2 design chart (steel grade S500)
(c) Results from proposed algorithm superimposed over the design chart

9.2 Example 2

This is an example presented by Chen et al. [2], which invokes the polygonal composite column cross section of Figure 8. The cross section consists of a concrete core, an asymmetrically placed H – shaped steel section, 15 reinforcement bars of diameter 18mm and a circular opening.

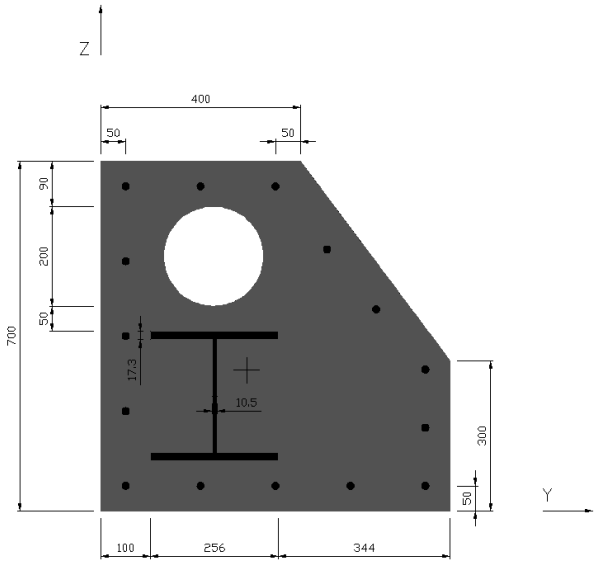

Figure 8. Composite column cross section

Chen et al. use a quasi – Newton method [10] to analyze the cross section. However, the convergence of the iterative process invoked by this algorithm cannot be guaranteed when dealing with large axial loads i.e. loads that approach the axial load capacity under pure compression. In order to ensure the stability of Chen's algorithm, the plastic centroid must be used as the origin of the Cartesian system. For an arbitrary cross section, the plastic centroid can be calculated as follows:

$$Y_{pc} = \frac{Y_c \cdot A_c \cdot f_{cc} \big/ \gamma_c + Y_s \cdot A_s \cdot f_s \big/ \gamma_s + Y_r \cdot A_r \cdot f_r \big/ \gamma_r}{A_c \cdot f_{cc} \big/ \gamma_c + A_s \cdot f_s \big/ \gamma_s + A_r \cdot f_r \big/ \gamma_r}$$
$$Z_{pc} = \frac{Z_c \cdot A_c \cdot f_{cc} \big/ \gamma_c + Z_s \cdot A_s \cdot f_s \big/ \gamma_s + Z_r \cdot A_r \cdot f_r \big/ \gamma_r}{A_c \cdot f_{cc} \big/ \gamma_c + A_s \cdot f_s \big/ \gamma_s + A_r \cdot f_r \big/ \gamma_r} \quad (14)$$

where, A_c, A_r, A_s are the total areas of concrete, reinforcing bars and structural steel respectively; f_{cc}, f_r, f_s are the respective characteristic strengths; γ_{cc}, γ_r, γ_s are the respective partial safety factors, Y_c, Z_c, Y_r, Z_r, Y_s, Z_s, are the coordinates of the respective centroids. In this case, the coordinates of the plastic centroid with respect to the bottom left corner are [2] Y_{pc}=292.2mm, Z_{pc}=281.5mm.

The stress – strain curve for concrete (CEC 1994) which consists of a parabolic and a linear (horizontal) part was used in the calculation, with $f_{cc}=0.85 \cdot f_{ck}/\gamma_c$, ε_0=0.002 and ε_{cu}=0.0035. The Young modulus for all steel sections was 200GPa while the maximum strain was $\varepsilon_u=\pm 0.010$.

The characteristic strengths and partial safety factors for concrete, structural steel and reinforcement bars were taken as follows:

$$f_{ck} = 30MPa, \gamma_c = 1.5$$
$$f_s = 355MPa, \gamma_s = 1.1$$
$$f_y = 460MPa, \gamma_r = 1.15$$

The analysis was carried out with an angle step of 5 degrees and an initial curvature step of 1e-06.

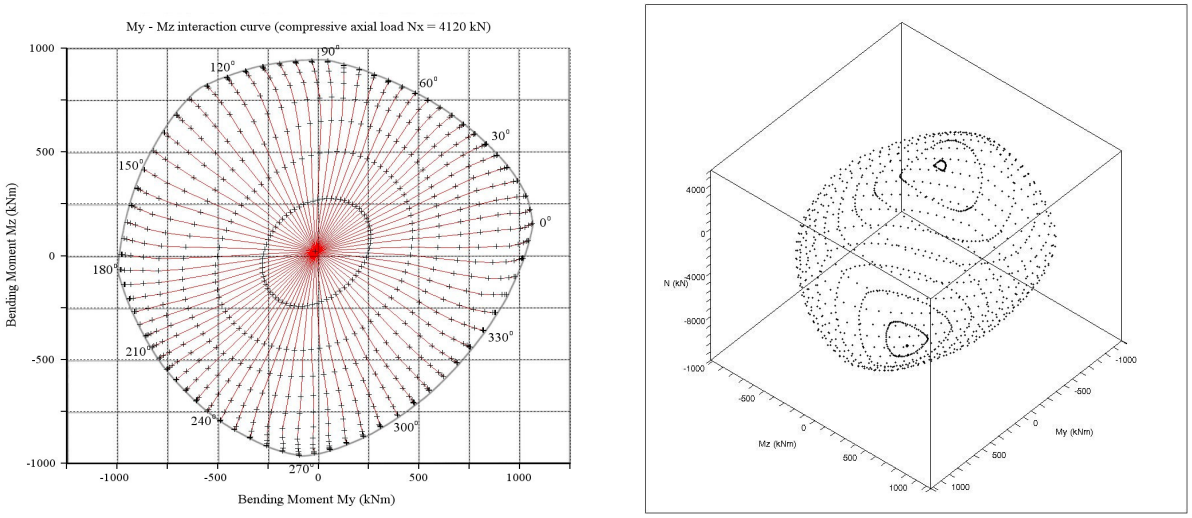

(a) (b)

Figure 9. (a) Interaction curve for compressive axial load 4120 kN
(b) Complete failure surface

Figure 9a shows the interaction curve produced by the proposed algorithm for compressive axial load 4120kN. The image is superimposed over the results taken from [2]; it is obvious that the curves almost coincide. The same figure also shows the paths of the analyses and the directions of the neutral axes that correspond to each spike. Note that the data for each spike becomes denser near failure; this is because the curvature step is decreased in order to achieve accuracy. By repeating this procedure for various axial loads we obtain the complete failure surface of Figure 9b.

9.3 Example 3

In this example, the versatility of the proposed algorithm is demonstrated. The task is to check the maximum bending moment capacity of a bolted connection of two circular tubes of diameter/width 1520/22mm and 1400/12.7mm respectively. The connection is implemented by means of two circular flanges and 24 bolts arranged in circle. The flanges are reinforced externally by dense out – of – plane triangular steel elements

(gussets), as shown in the figures.

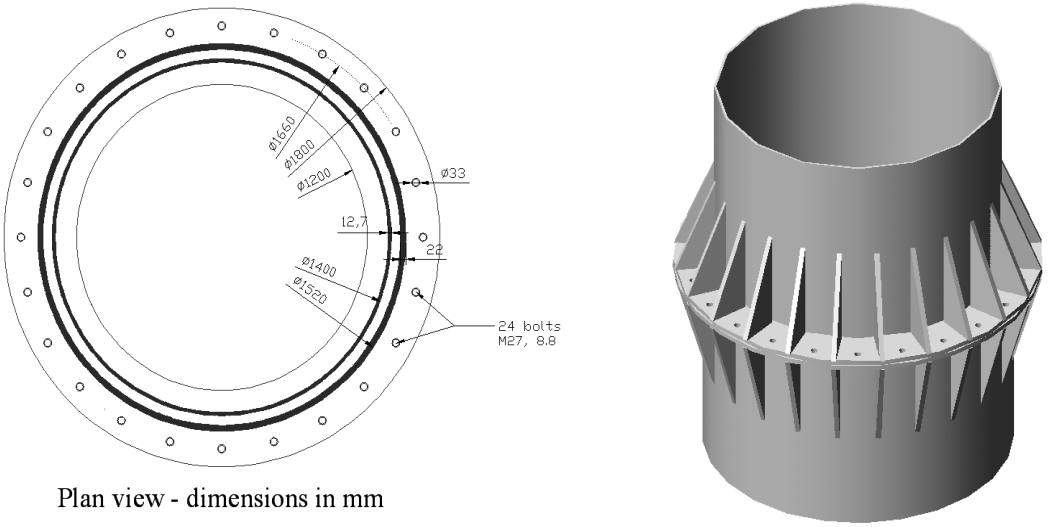

Figure 10. (a) Plan view of the proposed connection
(b) 3D view of the proposed connection

We assume that the flanges are rigid by virtue of the triangular steel elements. However, the rigidity does not extend to the inner circle of the two flanges; we assume that the effective rigid ring has a width of 187mm, as shown in Figure 11a.

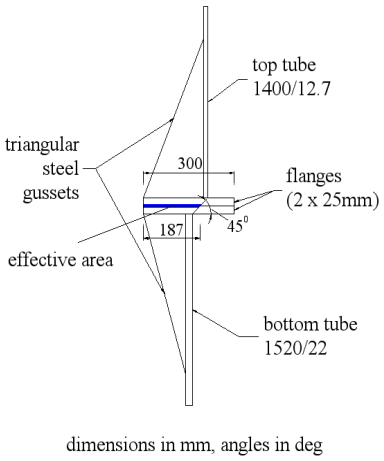

Property	Value
Bottom tube, external diameter	1520mm
Bottom tube, thickness	22mm
Top tube, external diameter	1400mm
Top tube, thickness	12.7mm
Flange, external diameter	1800mm
Flange, internal diameter	1200mm
Flange, thickness	25mm
Steel grade	S235
Number of bolts	24
Bolt size	M27
Bolt quality	8.8
Bolts arrangement, circle diameter	1660mm
Bolts hole, circle diameter	33mm
Axial load (compressive)	325kN

(b)

Figure 11. (a) Section of the proposed connection (b) Table of properties

Two materials are now defined: the flanges behave linearly in compression up to yield strength i.e. 235MPa/1.10=213.636MPa; however they do not exhibit tensile strength. We expect the flanges not to yield i.e. the failure should occur because of the bolts.

We assume that the bolts (quality 8.8) exhibit a bilinear behavior. The first linear segment extends in tension up to yield strength i.e. 640MPa/1.25=512MPa; the second linear segment extends up to ultimate strength defined by EC3, i.e. 0.9·800MPa/1.25=576MPa; however they do not exhibit compressive strength.

Young modulus is taken equal to 200GPa for all cases. Of course, the material properties may be defined otherwise and may also include parabolic or cubic segments, subject to the user's needs or assumptions.

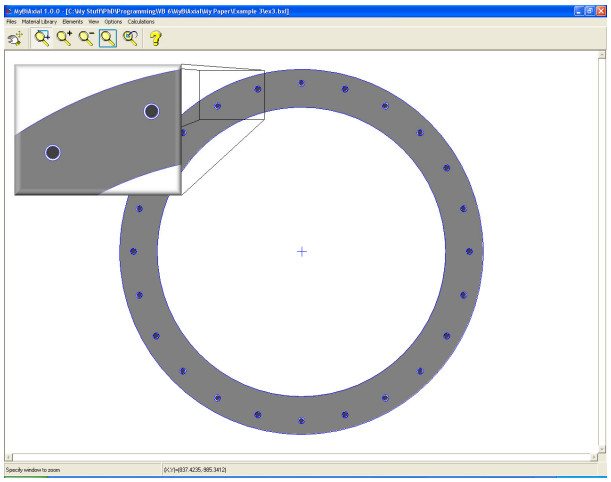

(a)

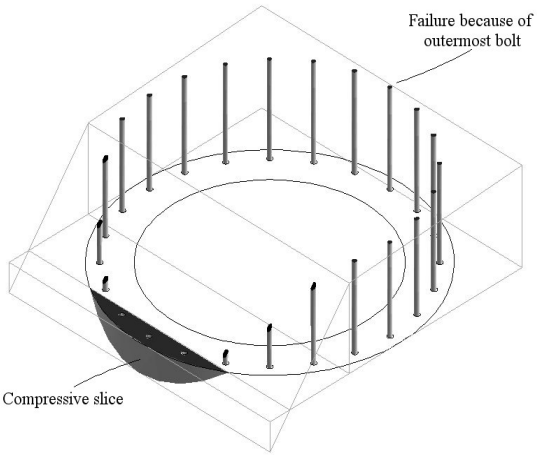

(b)

Figure 12. (a) Example 3 in MyBiAxial computer program
(b) 3D view of stress solids - verification of results using CAD software

For an axial (compressive) load of N_{Xc}=325kN, the algorithm yields the following results: curvature $k=6.223\cdot10^{-6}$, strain at the origin $\varepsilon_0=4.751\cdot10^{-3}$, ultimate bending moment at failure M_{Yc}=6466.160kNm. The minimum strain for the flanges is $\varepsilon_{min,flanges}=-8.493\cdot10^{-4}$; therefore, the flanges do not yield, as assumed from the beginning. The failure occurs because of the outermost bolt, which reaches the maximum strain of $\varepsilon_{max,bolts}=\pm0.010$.

Based on these data, the stress solids were created using CAD software (Figure 12b). The results are summarized in Table 2; the sum of the volume of all stress solids is equal to the axial load and the sum of all moments is equal to the result obtained from the proposed algorithm.

Element	Volume (or Force, kN)	Y_c Coordinate of Centroid (mm)	Bending Moment M_{Yc} (kNm)
Flange	-5876.257	-842.452	4950.463
Bolts #11 (· 2)	63.718	-717.782	-45.735
Bolts #10 (· 2)	251.698	-586.641	-147.656
Bolts #9 (· 2)	496.678	-414.869	-206.056
Bolts #8 (· 2)	594.712	-214.815	-127.753
Bolts #7 (· 2)	607.880	0.000	0.000
Bolts #6 (· 2)	621.048	214.824	133.416
Bolts #5 (· 2)	633.318	415.004	262.830
Bolts #4 (· 2)	643.855	586.903	377.880
Bolts #3 (· 2)	651.940	718.805	468.618
Bolts #2 (· 2)	657.023	801.723	526.750
Bolt #1 (· 1)	329.378	830.004	273.385
Sums :	-325.009		6466.141

Table 2. Computed results from CAD software

9.4 Example 4

In this example, the task is to calculate the maximum bending moment capacity of a rigid footing (Figure 13). We assume that the footing is placed over sand modeled with independent springs (Winkler); failure occurs when stress exceeds a predefined maximum value.

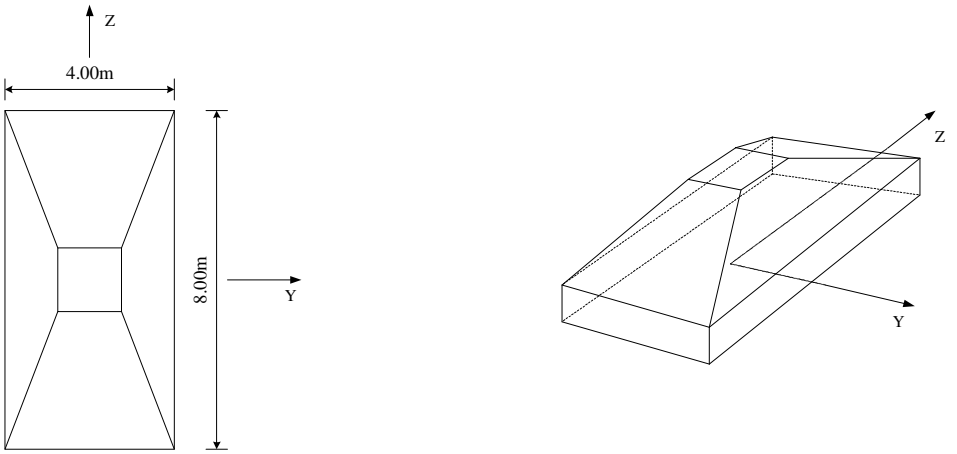

(a) (b)

Figure 13. (a) Plan view of rigid footing (b) 3D view of rigid footing

Property	Value
Rigid footing, length	8.00m
Rigid footing, width	4.00m
Axial load (compressive)	1300kN
Sand, k	20kPa/mm
Sand, maximum stress	250kPa

Table 3. Properties

We assume that sand behaves linearly in compression up to a maximum stress of 250kPa with a subgrade modulus k_s=20kPa/mm (maximum settlement 12.5mm); also, it does not exhibit tensile strength. Note that linear behavior is not obligatory; moreover, in this case, the stresses are expressed with respect to settlement instead of strain.

For an axial (compressive) load of N_{Xc}=1300kN, the algorithm yields the following results: curvature k=4.808, settlement at the origin ε_0=6.731mm, ultimate bending moment at failure M_{Yc}=4073.331kNm. The failure occurs because the sand reaches the maximum stress capacity of 250kPa (Figure 13a). The results are easily verifiable (equation (15))

$$\begin{aligned} N &= \frac{1}{2}\cdot 250KPa\cdot 2.60m\cdot 4.00m = 1300kN \\ M &= 1300kN\cdot\left(1.40m+\frac{2}{3}\cdot 2.60m\right) = 4073.333kNm \end{aligned} \tag{15}$$

As a step further, we may want to restrict the length of the ineffective area of the footing. This is achieved easily by applying a restriction similar to that of "Point C" of EC 2, which is described in Example 1. For example, we demand that the settlement at distance ½ h from the most compressed point i.e. at the middle of the footing, to be less than or equal to zero. In this way, more than half of the footing is always in contact with the sand. In this case and for the same axial (compressive) load of N_{Xc}=1300kN, the algorithm yields the following results: curvature k=2.031, settlement at the origin ε_c=0.000mm, ultimate bending moment at failure M_{Yc}=3466.667kNm (Figure 13b). Again, the results are easily verifiable (equation (16)):

$$\begin{aligned} N &= \frac{1}{2}\cdot 162.5KPa\cdot 4.00m\cdot 4.00m = 1300kN \\ M &= 1300kN\cdot\left(\frac{2}{3}\cdot 4.00m\right) = 3466.666kNm \end{aligned} \tag{16}$$

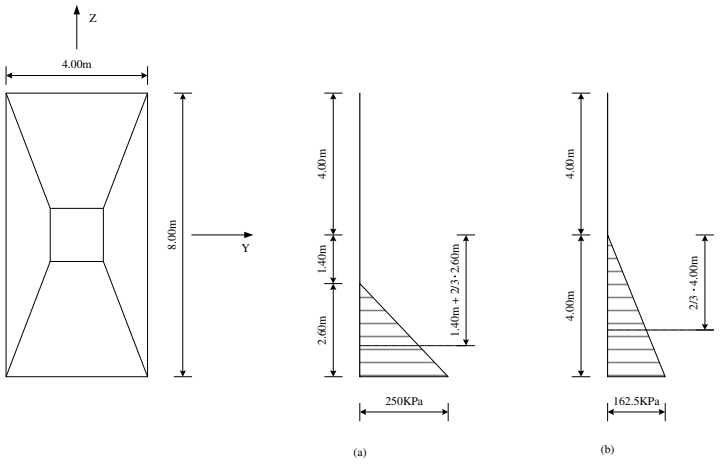

Figure 14. (a) Stresses with no restriction (compressive axial load 1300kN)
(b) Stresses with restriction at midpoint of rigid footing (compressive axial load 1300kN)

10 CONCLUSIONS

A generic algorithm for the analysis of arbitrary cross sections under biaxial bending and axial load is presented. The algorithm has some unique characteristics compared to the literature. The cross section is described by curvilinear polygons, i.e. closed polygons with straight or curved edges; the material stress – strain diagrams are fully user – defined as piecewise functions of polynomial segments; the integration of the stress field is analytical even for curved objects. Apart from producing interaction curves and failure surfaces, the algorithm can be used for the calculation of the deformed state of the cross section under given loads.

The algorithm has proved to be very stable and fast while providing analytical results. Moreover, it is a versatile tool that can be used for many purposes.

APPENDIX

Referring to the curvilinear trapezoid of Figure 15, there are nine possible combinations of curved or straight edges. The parameters identifying the type of edge are D_5, D_6 as shown in the figure.

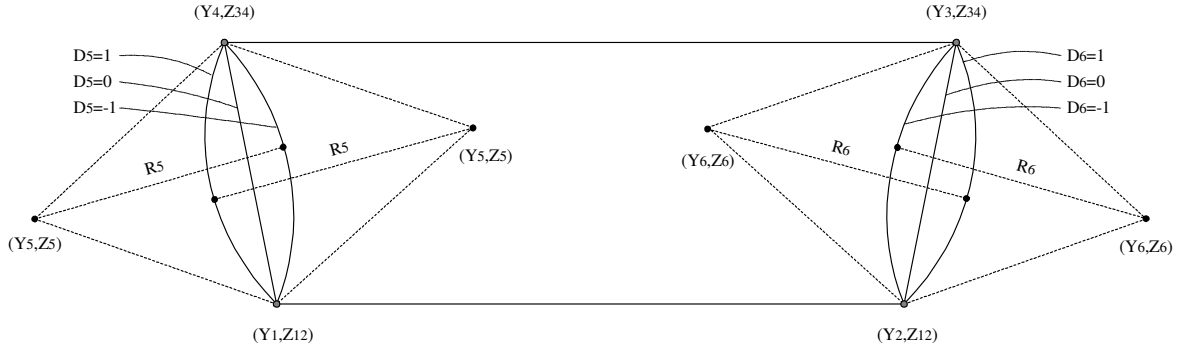

Figure 15. Curvilinear trapezoid

The integral for the case of straight edges is always calculated. Assuming that $z_{34}>z_{12}$ we have:

$$L_{14} = \frac{y_4 - y_1}{z_{34} - z_{12}}$$
$$L_{23} = \frac{y_3 - y_2}{z_{34} - z_{12}} \tag{17}$$

$$I^{j}_{(0,n)} = \frac{1}{n+2} \cdot (L_{23} - L_{14}) \cdot ({z_{34}}^{n+2} - {z_{12}}^{n+2}) + \frac{1}{n+1} \cdot (y_2 - L_{23} \cdot z_{12} - y_1 + L_{14} \cdot z_{12}) \cdot ({z_{34}}^{n+1} - {z_{12}}^{n+1}) \tag{18}$$

$$A = \frac{1}{2}\cdot\left(L_{23}{}^2 - L_{14}{}^2\right)$$
$$B = (y_2 - L_{23}\cdot z_{12})\cdot L_{23} - (y_1 - L_{14}\cdot z_{12})\cdot L_{14} \tag{19}$$
$$C = \frac{1}{2}\cdot\left((y_2 - L_{23}\cdot z_{12})^2 - (y_1 - L_{14}\cdot z_{12})^2\right)$$

$$I^j_{(1,n)} = \frac{1}{n+3}\cdot A\cdot\left(z_{34}{}^{n+3} - z_{12}{}^{n+3}\right) + \frac{1}{n+2}\cdot B\cdot\left(z_{34}{}^{n+2} - z_{12}{}^{n+2}\right) + \frac{1}{n+1}\cdot C\cdot\left(z_{34}{}^{n+1} - z_{12}{}^{n+1}\right) \tag{20}$$

If there are curved edges, the integral for the slice is calculated and it is added to or subtracted from the corresponding integral of the trapezoid. This is not required when the left and right edges are straight lines (which is the common case). We will examine the case for D_5 equal to 1. The generic solution involves the hypergeometric function; however, since we are interested in specific integrals, we will calculate them explicitly. For D_5=1:

$$A_{12} = \arcsin\left(\frac{z_5 - z_{12}}{R_5}\right)$$
$$A_{34} = \arcsin\left(\frac{z_5 - z_{34}}{R_5}\right) \tag{21}$$

$$S_{12} = \sqrt{(R_5{}^2 + 2\cdot z_5\cdot z_{12} - z_5{}^2 - z_{12}{}^2)}$$
$$S_{34} = \sqrt{(R_5{}^2 + 2\cdot z_5\cdot z_{34} - z_5{}^2 - z_{34}{}^2)} \tag{22}$$

$$I_{(0,0)} = -y_1\cdot z_{12} + \frac{1}{2}\cdot L_{14}\cdot z_{12}{}^2 + y_5\cdot z_{12} - \frac{1}{2}\cdot S_{12}\cdot z_{12} + \frac{1}{2}\cdot S_{12}\cdot z_5 + \frac{1}{2}\cdot R_5{}^2\cdot A_{12} + y_1\cdot z_{34} + \frac{1}{2}\cdot L_{14}\cdot z_{34}{}^2 -$$
$$-L_{14}\cdot z_{34}\cdot z_{12} - y_5\cdot z_{34} + \frac{1}{2}\cdot S_{34}\cdot z_{34} - \frac{1}{2}\cdot S_{34}\cdot z_5 - \frac{1}{2}\cdot R_5{}^2\cdot A_{34} \tag{23}$$

$$I_{(0,1)} = \frac{1}{3}\cdot S_{12}{}^3 - \frac{1}{2}\cdot y_1\cdot z_{12}{}^2 - \frac{1}{2}\cdot S_{12}\cdot z_5\cdot z_{12} + \frac{1}{2}\cdot y_5\cdot z_{12}{}^2 + \frac{1}{2}\cdot S_{12}\cdot z_5{}^2 + \frac{1}{2}\cdot z_5\cdot R_5{}^2\cdot A_{12} + \frac{1}{6}\cdot L_{14}\cdot z_{12}{}^3 - \frac{1}{3}\cdot S_{34}{}^3 +$$
$$+\frac{1}{2}\cdot z_5\cdot S_{34}\cdot z_{34} - \frac{1}{2}\cdot S_{34}\cdot z_5{}^2 - \frac{1}{2}\cdot z_5\cdot R_5{}^2\cdot A_{34} + \frac{1}{3}\cdot L_{14}\cdot z_{34}{}^3 + \frac{1}{2}\cdot z_{34}{}^2\cdot y_1 - \frac{1}{2}\cdot z_{34}{}^2\cdot L_{14}\cdot z_{12} - \frac{1}{2}\cdot z_{34}{}^2\cdot y_5 \tag{24}$$

$$I_{(0,2)} = \frac{1}{8}\cdot R_5{}^2\cdot S_{12}\cdot z_5 - \frac{1}{2}\cdot S_{12}\cdot z_5{}^2\cdot z_{12} - \frac{1}{8}\cdot R_5{}^2\cdot S_{12}\cdot z_{12} + \frac{1}{8}\cdot R_5{}^4\cdot A_{12} - \frac{1}{8}\cdot R_5{}^4\cdot A_{34} + \frac{1}{3}\cdot z_{34}{}^3\cdot y_1 - \frac{1}{3}\cdot z_{34}{}^3\cdot y_5 +$$
$$+\frac{1}{4}\cdot L_{14}\cdot z_{34}{}^4 - \frac{1}{4}\cdot z34\cdot S_{34}{}^3 - \frac{5}{12}\cdot z_5\cdot S_{34}{}^3 - \frac{1}{2}\cdot S_{34}\cdot z_5{}^3 + \frac{1}{12}\cdot L_{14}\cdot z_{12}{}^4 - \frac{1}{3}\cdot y_1\cdot z_{12}{}^3 + \frac{1}{2}\cdot z_5{}^2\cdot R_5{}^2\cdot A_{12} +$$
$$+\frac{1}{2}\cdot S_{12}\cdot z_5{}^3 + \frac{1}{4}\cdot S_{12}{}^3\cdot z_{12} + \frac{5}{12}\cdot z_5\cdot S_{12}{}^3 - \frac{1}{2}\cdot z_5{}^2\cdot R_5{}^2\cdot A_{34} + \frac{1}{8}\cdot R_5{}^2\cdot S_{34}\cdot z_{34} - \frac{1}{8}\cdot R_5{}^2\cdot S_{34}\cdot z_5 -$$
$$-\frac{1}{3}\cdot z_{34}{}^3\cdot L_{14}\cdot z_{12} + \frac{1}{2}\cdot z_5{}^2\cdot S_{34}\cdot z_{34} + \frac{1}{3}\cdot y_5\cdot z_{12}{}^3 \tag{25}$$

$$I_{(0,3)} = -\frac{1}{2}\cdot z_5{}^3\cdot R_5{}^2\cdot A_{34} - \frac{3}{8}\cdot z_5\cdot R_5{}^4\cdot A_{34} - \frac{1}{2}\cdot S_{12}\cdot z_5{}^3\cdot z_{12} + \frac{3}{8}\cdot R_5{}^2\cdot S_{12}\cdot z_5{}^2 + \frac{1}{2}\cdot z_5{}^3\cdot S_{34}\cdot z_{34} - \frac{3}{8}\cdot R_5{}^2\cdot S_{34}\cdot z_5{}^2 +$$
$$+\frac{7}{20}\cdot z_5\cdot S_{12}{}^3\cdot z_{12} - \frac{1}{4}\cdot z_{34}{}^4\cdot y_5 + \frac{3}{8}\cdot z_5\cdot R_5{}^4\cdot A_{12} + \frac{1}{2}\cdot z_5{}^3\cdot R_5{}^2\cdot A_{12} + \frac{1}{20}\cdot L_{14}\cdot z_{12}{}^5 - \frac{1}{4}\cdot y_1\cdot z_{12}{}^4 + \frac{1}{4}\cdot y_5\cdot z_{12}{}^4 +$$
$$+\frac{1}{5}\cdot S_{12}{}^3\cdot z_{12}{}^2 + \frac{2}{15}\cdot R_5{}^2\cdot S_{12}{}^3 + \frac{9}{20}\cdot z_5{}^2\cdot S_{12}{}^3 - \frac{2}{15}\cdot R_5{}^2\cdot S_{34}{}^3 - \frac{1}{5}\cdot z_{34}{}^2\cdot S_{34}{}^3 - \frac{9}{20}\cdot z_5{}^2\cdot S_{34}{}^3 - \frac{3}{8}\cdot R_5{}^2\cdot S_{12}\cdot z_5\cdot z_{12} -$$
$$-\frac{7}{20}\cdot z_5\cdot z_{34}\cdot S_{34}{}^3 + \frac{1}{2}\cdot S_{12}\cdot z_5{}^4 - \frac{1}{2}\cdot S_{34}\cdot z_5{}^4 - \frac{1}{4}\cdot z_{34}{}^4\cdot L_{14}\cdot z_{12} + \frac{1}{4}\cdot z_{34}{}^4\cdot y_1 + \frac{1}{5}\cdot L_{14}\cdot z_{34}{}^5 + \frac{3}{8}\cdot z_5\cdot R_5{}^2\cdot S_{34}\cdot z_{34} \tag{26}$$

$$
\begin{aligned}
I_{(0,4)} = & -\frac{3}{4}\cdot z_5^{\,2}\cdot R_5^{\,4}\cdot A_{34} - \frac{1}{2}\cdot z_5^{\,4}\cdot R_5^{\,2}\cdot A_{34} + \frac{1}{16}\cdot R_5^{\,4}\cdot S_{34}\cdot z_{34} - \frac{3}{4}\cdot R_5^{\,2}\cdot S_{34}\cdot z_5^{\,3} + \frac{1}{2}\cdot z_5^{\,4}\cdot S_{34}\cdot z_{34} - \\
& - \frac{1}{16}\cdot R_5^{\,4}\cdot S_{12}\cdot z_{12} + \frac{1}{16}\cdot R_5^{\,4}\cdot S_{12}\cdot z_5 - \frac{1}{2}\cdot S_{12}\cdot z_5^{\,4}\cdot z_{12} + \frac{3}{4}\cdot R_5^{\,2}\cdot S_{12}\cdot z_5^{\,3} + \frac{3}{4}\cdot z_5^{\,2}\cdot R_5^{\,4}\cdot A_{12} + \\
& + \frac{1}{2}\cdot z_5^{\,4}\cdot R_5^{\,2}\cdot A_{12} - \frac{1}{8}\cdot R_5^{\,2}\cdot z_{34}\cdot S_{34}^{\,3} - \frac{49}{120}\cdot z_5\cdot R_5^{\,2}\cdot S_{34}^{\,3} - \frac{3}{10}\cdot z_5\cdot z_{34}^{\,2}\cdot S_{34}^{\,3} - \frac{2}{5}\cdot z_5^{\,2}\cdot z_{34}\cdot S_{34}^{\,3} + \\
& + \frac{3}{10}\cdot z_5\cdot S_{12}^{\,3}\cdot z_{12}^{\,2} + \frac{49}{120}\cdot z_5\cdot R_5^{\,2}\cdot S_{12}^{\,3} + \frac{1}{8}\cdot R_5^{\,2}\cdot S_{12}^{\,3}\cdot z_{12} + \frac{2}{5}\cdot z_5^{\,2}\cdot S_{12}^{\,3}\cdot z_{12} - \frac{1}{16}\cdot R_5^{\,4}\cdot S_{34}\cdot z_5 - \\
& - \frac{3}{4}\cdot R_5^{\,2}\cdot S_{12}\cdot z_5^{\,2}\cdot z_{12} + \frac{3}{4}\cdot z_5^{\,2}\cdot R_5^{\,2}\cdot S_{34}\cdot z_{34} - \frac{1}{16}\cdot R_5^{\,6}\cdot A_{34} - \frac{1}{6}\cdot z_{34}^{\,3}\cdot S_{34}^{\,3} - \frac{7}{15}\cdot z_5^{\,3}\cdot S_{34}^{\,3} + \\
& + \frac{1}{5}\cdot z_{34}^{\,5}\cdot y_1 - \frac{1}{5}\cdot z_{34}^{\,5}\cdot y_5 + \frac{1}{6}\cdot S_{12}^{\,3}\cdot z_{12}^{\,3} + \frac{7}{15}\cdot z_5^{\,3}\cdot S_{12}^{\,3} - \frac{1}{2}\cdot S_{34}\cdot z_5^{\,5} - \frac{1}{5}\cdot z_{34}^{\,5}\cdot L_{14}\cdot z_{12} + \\
& + \frac{1}{6}\cdot L_{14}\cdot z_{34}^{\,6} + \frac{1}{2}\cdot S_{12}\cdot z_5^{\,5} + \frac{1}{16}\cdot R_5^{\,6}\cdot A_{12} + \frac{1}{30}\cdot L_{14}\cdot z_{12}^{\,6} - \frac{1}{5}\cdot y_1\cdot z_{12}^{\,5} + \frac{1}{5}\cdot y_5\cdot z_{12}^{\,5}
\end{aligned}
\tag{27}
$$

$$
\begin{aligned}
I_{(1,0)} = & -\frac{1}{2}\cdot y_5\cdot R_5^{\,2}\cdot A_{34} + \frac{1}{2}\cdot y_5\cdot R_5^{\,2}\cdot A_{12} - \frac{1}{2}\cdot y_5\cdot S_{34}\cdot z_5 + \frac{1}{2}\cdot y_5\cdot S_{34}\cdot z_{34} + \frac{1}{2}\cdot y_5\cdot S_{12}\cdot z_5 - \frac{1}{2}\cdot y_5\cdot S_{12}\cdot z_{12} + \\
& + \frac{1}{6}\cdot L_{14}^{\,2}\cdot z_{34}^{\,3} - \frac{1}{2}\cdot y_1^{\,2}\cdot z_{12} + \frac{1}{2}\cdot y_1^{\,2}\cdot z_{34} - \frac{1}{2}\cdot L_{14}^{\,2}\cdot z_{34}^{\,2}\cdot z_{12} + \frac{1}{2}\cdot L_{14}^{\,2}\cdot z_{34}\cdot z_{12}^{\,2} + \frac{1}{2}\cdot y_1\cdot L_{14}\cdot z_{34}^{\,2} - \frac{1}{6}\cdot L_{14}^{\,2}\cdot z_{12}^{\,3} - \\
& - \frac{1}{2}\cdot z_{12}\cdot z_5^{\,2} + \frac{1}{2}\cdot y_5^{\,2}\cdot z_{12} + \frac{1}{2}\cdot z_5\cdot z_{12}^{\,2} + \frac{1}{2}\cdot z_{12}\cdot R_5^{\,2} + \frac{1}{6}\cdot z_{34}^{\,3} - \frac{1}{6}\cdot z_{12}^{\,3} + \frac{1}{6}\cdot L_{14}\cdot y_1\cdot z_{12}^{\,2} - y_1\cdot L_{14}\cdot z_{34}\cdot z_{12} - \\
& - \frac{1}{2}\cdot R_5^{\,2}\cdot z_{34} - \frac{1}{2}\cdot z_{34}^{\,2}\cdot z_5 + \frac{1}{2}\cdot z_5^{\,2}\cdot z_{34} - \frac{1}{2}\cdot y_5^{\,2}\cdot z_{34}
\end{aligned}
\tag{28}
$$

$$
\begin{aligned}
I_{(1,1)} = & \frac{1}{3}\cdot y_5\cdot S_{12}^{\,3} + \frac{1}{4}\cdot z_{34}^{\,2}\cdot L_{14}^{\,2}\cdot z_{12}^{\,2} + \frac{1}{3}\cdot L_{14}\cdot z_{34}^{\,3}\cdot y_1 - \frac{1}{3}\cdot L_{14}^{\,2}\cdot z_{34}^{\,3}\cdot z_{12} - \frac{1}{2}\cdot y_5\cdot z_5\cdot R_5^{\,2}\cdot A_{34} + \frac{1}{3}\cdot z_5\cdot z_{12}^{\,3} + \\
& + \frac{1}{4}\cdot R_5^{\,2}\cdot z_{12}^{\,2} - \frac{1}{4}\cdot z_5^{\,2}\cdot z_{12}^{\,2} - \frac{1}{24}\cdot L_{14}^{\,2}\cdot z_{12}^{\,4} - \frac{1}{4}\cdot y_1^{\,2}\cdot z_{12}^{\,2} + \frac{1}{4}\cdot y_5^{\,2}\cdot z_{12}^{\,2} - \frac{1}{3}\cdot z_{34}^{\,3}\cdot z_5 - \frac{1}{8}\cdot z_{12}^{\,4} - \frac{1}{3}\cdot y_5\cdot S_{34}^{\,3} + \\
& + \frac{1}{8}\cdot z_{34}^{\,4} + \frac{1}{4}\cdot z_{34}^{\,2}\cdot y_1^{\,2} - \frac{1}{4}\cdot z_{34}^{\,2}\cdot y_5^{\,2} - \frac{1}{4}\cdot z_{34}^{\,2}\cdot R_5^{\,2} + \frac{1}{4}\cdot z_{34}^{\,2}\cdot z_5^{\,2} + \frac{1}{2}\cdot y_5\cdot z_5\cdot S_{34}\cdot z_{34} - \frac{1}{2}\cdot y_5\cdot S_{12}\cdot z_5\cdot z_{12} - \\
& - \frac{1}{2}\cdot z_{34}^{\,2}\cdot y_1\cdot L_{14}\cdot z_{12} + \frac{1}{2}\cdot y_5\cdot S_{12}\cdot z_5^{\,2} + \frac{1}{6}\cdot L_{14}\cdot y_1\cdot z_{12}^{\,3} + \frac{1}{2}\cdot y_5\cdot z_5\cdot R_5^{\,2}\cdot A_{12} + \frac{1}{8}\cdot L_{14}^{\,2}\cdot z_{34}^{\,4} - \frac{1}{2}\cdot y_5\cdot S_{34}\cdot z_5^{\,2}
\end{aligned}
\tag{29}
$$

REFERENCES

[1] Bonet, J.L., Romero, M.L., Miguel, P.F., Fernandez, M.A. (2004), "A fast stress integration algorithm for reinforced concrete sections with axial loads and biaxial bending", Computers and Structures 82 213-225

[2] Chen, S. F., Teng, J. G., Chan, S. L. (2001), "Design of biaxially loaded short composite columns of arbitrary cross section", J. Struct Engng, ASCE; 127(6):678-685.

[3] De Vivo, L, Rosati, L. (1998), "Ultimate strength analysis of reinforced concrete sections subject to axial force and biaxial bending", Comput. Methods Appl. Mech. Engrg. 166:261-287.

[4] Fafitis, A (2001), "Interaction surfaces of reinforced-concrete sections in biaxial bending", J Struct Engng, ASCE; 127(7):840-6

[5] Press, W. H., Teukolsky, S. A., Vetterling, W. T., Flannery, B. P. (2002), *Numerical recipes in C++: the art of scientific computing*, Cambridge University Press.

[6] Rodriguez, J. A., Aristizabal-Ochoa, J. Dario (1999), “Biaxial interaction diagrams for short RC columns of any cross section”, J Struct Engng, ASCE; 125(6):672-683.

[7] Rodriguez, J. A., Aristizabal-Ochoa, J. Dario (2001), “M-P-φ diagrams for reinforced, partially and fully prestressed concrete sections under biaxial bending and axial load”, J Struct Engng, ASCE; 127(7):763-773.

[8] Rodriguez, J. A., Aristizabal-Ochoa, J. Dario (2001), “Reinforced, partially and fully prestressed concrete columns under biaxial bending and axial load”, J Struct Engng, ASCE; 127(7):774-783.

[9] Sfakianakis, M. G. (2002), “Biaxial bending with axial force of reinforced, composite and repaired concrete sections of arbitrary shape by fiber model and computer graphics”, Advances in Engineering Software 33 227 - 242.

[10] Yen, J. Y. R. (1991), “Quasi-Newton method for reinforced concrete column analysis and design”, J Struct Engng, ASCE; 117(3):657-666.